A Constant Voltage WPT System for AM-Modulated Implant Neural Stimulation

Zhiyang Cao , Shicong Gui , Chujia Xu , Rui Zhong , Zhaotan Lin , Yubo Li *

Posted Date: 1 July 2024

doi: 10.20944/preprints202407.0038.v1

Keywords: WPT; resonance inductive coupling; wireless neural stimulator; implant device

Article

A Constant Voltage WPT System for AM-Modulated Implant Neural Stimulation †

Zhiyang Cao [1,‡], Shicong Gui [2,‡], Chujia Xu [2], Rui Zhong [2], Zhaotan Lin [2] and Yubo Li [2,3*]

[1] College of Electrical Engineering, Zhejiang University, Hangzhou, 310027, China;
[2] College of Information Science and Electronic Engineering, Zhejiang University, Hangzhou, 310027, China
[3] International Joint Innovation Center, Zhejiang University, Haining, 314400, China
* Correspondence: lilinear@zju.edu.cn
† This paper is an extended version of our paper published in INGEP 2024.
‡ These authors contributed equally to this work.

Abstract: Resonance inductive coupling is widely used for wireless power transfer (WPT) in medical applications. In this paper, we analyze the LCL-compensated WPT structure and propose a novel constant voltage transmission system based on gain estimation, without any extra feedback from the receiver. The system is capable for implant neural stimulation where the load impedance and the coupling coefficient are both variable. Compared to existing methods for constant voltage transmission, our approach offers advantages in compact size and the compatibility with the industrial, scientific and medical (ISM) band. We validate the load-independent resonant characteristic and the feasibility of constant voltage transmission using an experimental prototype working at 6.78MHz. Finally, we discuss the structure of the implant stimulator and methods of applying the proposed WPT system.

Keywords: WPT; resonance inductive coupling; wireless neural stimulator; implant device

1. Introduction

Neural stimulation has long been practiced as an effective treatment for chronic diseases and pain. In recent years, advancements in electronic engineering have brought significant attention to implantable stimulators with wireless power transfer (WPT) capabilities.

Among a series of WPT techniques, resonance inductive coupling technology is most commonly employed for neural stimulation[1]. The basic principle is to utilize LC resonance characteristic to generate higher voltage or current and compensate the gain deduction caused by the enlarged gap. However, there are drawbacks of the traditional structure. The resonant frequency splits with varying coupling coefficient [2], and the voltage gain is affected by load impedance.

It is a popular direction for improvement to added compensation networks to the original circuit and form hybrid topologies. Numerous structures have been proposed, such as LCC[3–5], LCL[6,7] and others. Most of these topologies are designed for kW-level WPT[8] and are modeled at frequency around 100kHz. For medical use, however, the WPT systems work at several hundred kilohertz to a few megahertz to ensure more compact size and biocompatibility[1,9,10]. The parasite parameters like the stray capacitance become remarkable in this range, but are often neglected since they are trivial in lower frequency and in high-power system [3,4,11,12]. Additionally, researches from the perspective of power electronics typically focus on efficiency, which is not the top priority in low-power medical use. Therefore, the MRC structure should be remodeled and better tuned for medical applications.

For AM or ASK modulated implant stimulators[13], insensitivity to misalignment is crucial because relative movement between the transmitter and receiver may lead to varying coupling coefficient, and consequently, changes in received voltage amplitude. The transmitter should be able to monitor the received voltage and implement feedback control. Besides complex wireless communication, one solution is to track the resonant frequency to maintain constant voltage gain[14], yet the narrow ISM band strictly limit the adjustment range. Another approach is to adaptively

 doi:10.20944/preprints202407.0038.v1

compensate the MRC circuit by a selective impedance matching network[15], but it is only capable for discrete control and involves bulky relays.

The purpose of this paper is to analyze and design the LCL-compensated WPT structure for constant voltage transmission, primarily for medical use. Section 2 derives the characteristics of the structure by modeling the circuit and theoretically proves the feasibility of CV-WPT. Section 3 presents the experimental results, and Section 4 discusses the application methods.

2. Materials and Methods

The proposed LCL-compensated WPT structure is shown in Figure 1a. The coils with self-inductance L_1 and L_2 are coupled with mutual inductance $M = k\sqrt{L_1 L_2}$, where k denotes the coupling coefficient. R_L depicts the equivalent AC load. $R_L = 8R_{dc}/\pi^2$ when the output is rectified and filtered. The circuit is re-drawn as Figure 1b for analysis. R_1 and R_2 depict ESR of the coils. C_{p1} is split into C_{p11} and C_{p12} using the conclusion of Li et-al[12] to provide extra degree of freedom and achieve load-independent constant voltage transmission. Parasite capacitance of both coils are absorbed by C_{p1} and C_{p2}. The composited capacitance can be measured and tuned to ideal in practice, hence the parasite capacitance is neglected in analysis.

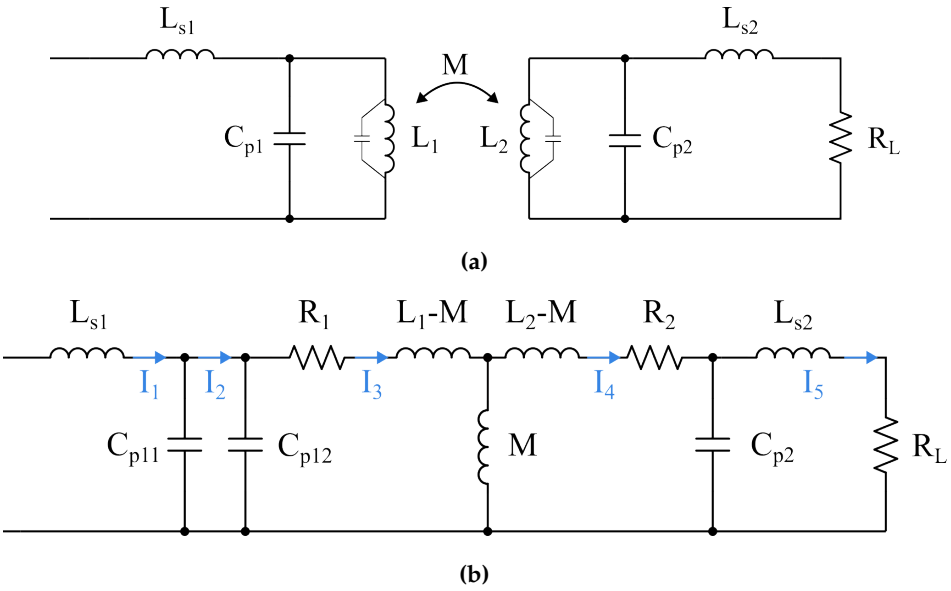

Figure 1. LCL-compensated WPT structure(a) and its equivalent circuit model(b)

2.1. Load-and-Matching-Independent Resonant Frequency

Denote the mesh currents in Figure 1b as I_1 to I_5, the KVL matrix is written as:

$$\begin{pmatrix} V_{in} \\ 0 \\ 0 \\ 0 \\ 0 \end{pmatrix} = \begin{pmatrix} jZ_1 & -\frac{1}{j\omega C_{p11}} & 0 & 0 & 0 \\ -\frac{1}{j\omega C_{p11}} & jZ_2 & -\frac{1}{j\omega C_{p12}} & 0 & 0 \\ 0 & -\frac{1}{j\omega C_{p12}} & jZ_3 & -j\omega M & 0 \\ 0 & 0 & -j\omega M & jZ_4 & -\frac{1}{j\omega C_{p2}} \\ 0 & 0 & 0 & -\frac{1}{j\omega C_{p2}} & jZ_5 + R_L \end{pmatrix} \begin{pmatrix} I_1 \\ I_2 \\ I_3 \\ I_4 \\ I_5 \end{pmatrix} = \mathbf{ZI} \tag{1}$$

In which jZ_1 to jZ_5 denote the complex impedance of each mesh. Parasite parameters are neglected temporarily. The voltage gain is then:

$$G_V = \frac{I_5 R_L}{V_{in}} = \mathbf{Z}^{-1}_{(5,1)} R_L \tag{2}$$

 doi:10.20944/preprints202407.0038.v1

$$G_V^{-1} = \frac{jC_{p2}C_{p11}C_{p12}}{MR_L} \cdot \begin{pmatrix} M^2Z_1Z_2Z_5\omega^4 - \frac{1}{C_{p11}^2}M^2Z_5\omega^2 - Z_1Z_2Z_3Z_4Z_5\omega^2 \\ -\frac{Z_1}{C_{p2}^2C_{p12}^2} - \frac{Z_3}{C_{p2}^2C_{p11}^2} + \frac{Z_1Z_4Z_5}{C_{p12}^2} + \frac{Z_3Z_4Z_5}{C_{p11}^2} + \frac{Z_1Z_2Z_3}{C_{p2}^2} \end{pmatrix}$$
$$+\frac{C_{p2}C_{p11}C_{p12}}{M}\left(M^2Z_1Z_2\omega^4 - Z_1Z_2Z_3Z_4\omega^2 - \frac{M^2\omega^2}{C_{p11}^2} + \frac{Z_1Z_4}{C_{p11}^2} + \frac{Z_3Z_4}{C_{p11}^2}\right) \tag{3}$$

It is obvious that when $Z_1 = Z_3 = Z_5 = 0$ there are $dG_V/dR_L = 0$ and $dG_V/dk = 0$, making the voltage gain irrelevant to both the load and the matching condition. To set this fully independent resonant frequency to be ω_0, the circuit should satisfies:

$$\begin{aligned} Z_1|_{\omega_0} &= \omega_0 L_{s1} - \frac{1}{\omega_0 C_{p11}} = 0 \\ Z_3|_{\omega_0} &= \omega_0 L_1 - \frac{1}{\omega_0 C_{p12}} = 0 \\ Z_5|_{\omega_0} &= \omega_0 L_{s2} - \frac{1}{\omega_0 C_{p2}} = 0 \end{aligned} \tag{4}$$

Merge Equation (3) and (4), the voltage gain at ω_0 only depends on k:

$$G_{V0} = -\frac{C_{p11}}{C_{p2}C_{p12}M\omega_0^2} = -\frac{1}{k} \cdot \frac{L_{s2}}{L_{s1}}\sqrt{\frac{L_1}{L_2}} \tag{5}$$

Equation (5) demonstrates that the LCL-compensated voltage gain is inversely proportional to $\sqrt{L_2/L_1}$ i.e. the "turns ratio" of an ideally-coupled transformer, which makes smaller receiving coil possible. Notice that the electromagnetic attenuation is neglected here. However, the loss becomes dominant in loosely-coupled condition and (5) no longer holds. Non-ideal parameters also restrict G_{V0} from increasing further with smaller k, which will be discussed later.

2.2. Online Estimation of Received Voltage

Although load-independent, voltage gain at ω_0 still varies with k. A feedback loop with information of received voltage V_{out} or the intermediate parameter k must be constructed. With LCL compensation, the needed signal can be extracted from the transmitting side. It avoids extra wireless communication from the receiver and enhances responding speed as well as robustness.

The input number is denoted as I_1 in Figure 1b. Let Equation (4) into Equation (1), I_1 at ω_0 is obtained:

$$I_1|_{\omega_0} \triangleq I_{10} = V_{in}\,\mathbf{Z}_{(1,1)}^{-1}\Big|_{\omega_0} = V_{in}\left(\frac{L_1^2L_{s2}^2}{R_LL_{s1}^2M^2} + j\frac{L_1^2\left(L_2 - L_{s2}\right) - M^2\left(L_{s1} + L_1\right)}{L_{s1}^2M^2\omega_0}\right) \tag{6}$$

Where the effect of R_L cannot be eliminated, but can be reduced to negligible. Let $A = \Re\left(I_1\right)$, $B = \Im\left(I_1\right)$, it is obvious that B is irrelevant to R_L. Then the effect of R_L on I_{10} is:

$$\frac{\mathrm{d}\left|I_{10}\right|}{\mathrm{d}R_L} = \frac{\mathrm{d}\sqrt{A^2+B^2}}{\mathrm{d}R_L} = \left(A^2+B^2\right)^{-\frac{1}{2}}A\frac{\mathrm{d}A}{\mathrm{d}R_L} = \frac{A}{|I_{10}|}\frac{\mathrm{d}A}{\mathrm{d}R_L}$$
$$= -\left(R_L + \frac{R_L^3}{V_{in}\omega_0} \cdot \frac{L_2L_{s1}^2k^2}{L_1^2L_{s2}^4}\left(L_1\left(L_2 - L_{s2}\right) - k^2L_2\left(L_1 + L_{s1}\right)\right)\right)^{-1} \tag{7}$$

$\mathrm{d}\left|I_{10}\right|/\mathrm{d}R_L$ diminishes with larger R_L. For KΩ-level load, the load adjustment rate can be further reduced by tuning the inductors ratio. Although a small L_2 is desired for more compact receiver, it is practical to have a larger L_{s1} and smaller L_{s2}. Notice that $L_2 \neq L_{s2}$, otherwise I_1 becomes irrelevant to k from Equation (6).

 doi:10.20944/preprints202407.0038.v1

At light load, Equation (6) becomes a function of k. $|I_{10}|$ monotonically deceases when $k < k_b$ and increases otherwise. The boundary k_b is obtained by:

$$\left.\frac{\mathrm{d}\,|I_{10}|}{\mathrm{d}k}\right|_{k=k_b} = \left.\frac{\mathrm{d}\sqrt{A^2+B^2}}{\mathrm{d}k}\right|_{k=k_b} = 0 \tag{8}$$

$$k_b = \frac{\sqrt{L_1L_2\left(L_2-L_{s2}\right)\left(L_1+L_{s1}\right)\left(\left(L_2-L_{s2}\right)^2+\frac{L_{s2}^4\omega_0^2}{R_L^2}\right)}}{L_2(L_2-L_{s2})(L_1+L_{s1})} \approx \sqrt{\frac{L_1\left(L_2-L_{s2}\right)}{L_2\left(L_1+L_{s1}\right)}} \tag{9}$$

When k_b is not within the working range, $|I_{10}|\,(k)$ is a always a monotonic function. Therefore the inverse function $\hat{k}(I_1)$ is single-valued and can be used to estimate k. Notice k_b is also where the maximum $\mathrm{d}\,|I_{10}|/\mathrm{d}R_L$ lies. So k_b should be put as far as possible from the possible range of k.

I_1 is extracted by measuring the amplitude of voltage across L_{s1}.

$$V_m = |I_{10}|\,\omega_0 L_{s1} \tag{10}$$

$$\hat{k} = \sqrt{-\frac{L_1V_{in}\left(V_mL_{s1}\left|L_2-L_{s2}\right|-V_{in}\left(L_1+L_{s1}\right)\left(L_2-L_{s2}\right)\right)}{L_2\left(L_1V_{in}+L_{s1}V_{in}+L_{s1}V_m\right)\left(L_1V_{in}+L_{s1}V_{in}-L_{s1}V_m\right)}} \tag{11}$$

Where V_{in} and V_m denotes the amplitude of the input and measured voltage respectively.

From Equation (5), the overall voltage gain at ω_0 is a single-valued function of k. Therefore for any measured $|V_m|$ there is only one corresponding G_{V0}. Hence the received voltage V_{out} can be estimated by Equation (12). The relationship between V_m, G_{V0} and k is shown in Figure 2.

$$\hat{V}_{out} = V_{in}G_{v0}\left(\hat{k}\left(V_m\right)\right) \tag{12}$$

Notice that Equation (11) and (12) only serve as a proof of the feasibility of the k estimation. It is recommended to plot $\hat{V}_{out}(V_m)$ in experiment to cover the disturbance of parasite parameters, which will be discussed later.

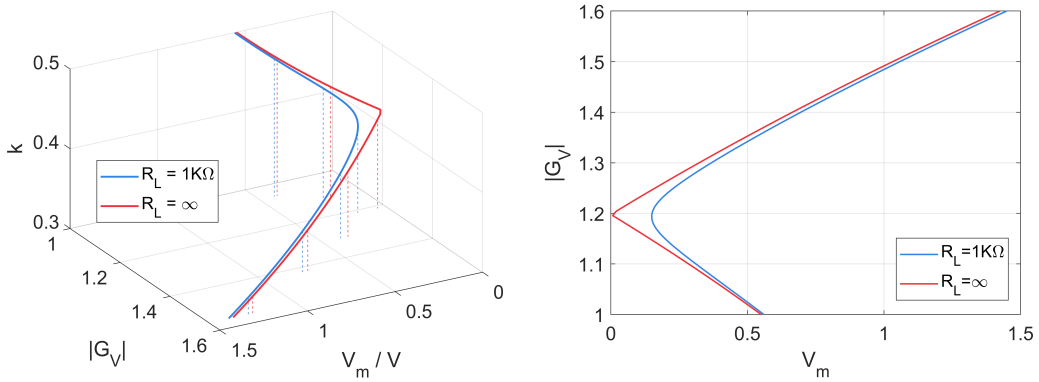

Figure 2. V_m-G-k relationship with $L_1 = L_2 = 1\mu$H, $L_{s1} = 1.22\mu$H, $L_{s2} = 0.61\mu$H at 13.56MHz

2.3. Minimization of Effect of Frequency Error

By selecting compensation component value as given in Equation (4), it is straightforward to demonstrate that ω_0 is the independent resonant frequency where $\Im\left(G_V\right) = 0$. However, ω_0 is not necessarily where the maximum voltage gain is achieved. A high Q-value in the LCL-compensated WPT circuit may results in significant overvoltage with minor deviations in frequency, posing risks especially in medical applications. Therefore, it is advisable to smoothen the gain curve around ω_0.

 doi:10.20944/preprints202407.0038.v1

To obtain G_V as a function of ω, expand Z_i in Equation (3):

$$G_V^{-1} = \begin{pmatrix} j\omega^5 & \omega^4 & j\omega^3 & \omega^2 & j\omega^1 & 1 \end{pmatrix} \mathbf{W} \tag{13}$$

Where $\mathbf{W}$ is the weight matrix of the polynomial function G_V^{-1}. It is omitted here for simplicity. The analytical solution of peaks of G_V^{-1} is hard to obtained, but it is still easy to investigate whether ω_0 is one of the solution. With the resonance characteristic that $\Im\left(G_V\right) = 0$, $\mathrm{d}\left|G_V\right|/\mathrm{d}\omega = 0$ as long as $\Re\left(\mathrm{d}G_V^{-1}/\mathrm{d}\omega\right) = 0$.

Obtain the derivative of Equation (13) to ω, then substitute ω with ω_0:

$$\begin{aligned} \left.\frac{\mathrm{d}G_V^{-1}}{\mathrm{d}\omega}\right|_{\omega_0} = & -\frac{2L_1^2L_{s2} - 2L_2L_1^2 + 2L_{s1}L_1L_{s2} - 2L_2L_{s1}L_1 + 2L_1M^2 + 4L_{s1}M^2}{L_1L_{s2}M\omega_0} \\ & + \frac{jL_1^2L_{s2} + jL_{s1}L_1L_{s2} + jL_{s1}M^2}{L_1R_LM} \end{aligned} \tag{14}$$

The real part of Equation (14) is variable with k. Thus ω_0 cannot be a static peak. However, when an average coupling coefficient k_0 is determined, the inductors can be tuned to minimize the gain slope around ω_0 as Equation (15). The effect is demonstrated in Figure 3.

$$\left(L_1 + L_{s1}\right)\left(L_{s2} - L_2\right) + k_0^2L_2\left(L_1 + 2L_{s1}\right) = 0 \tag{15}$$

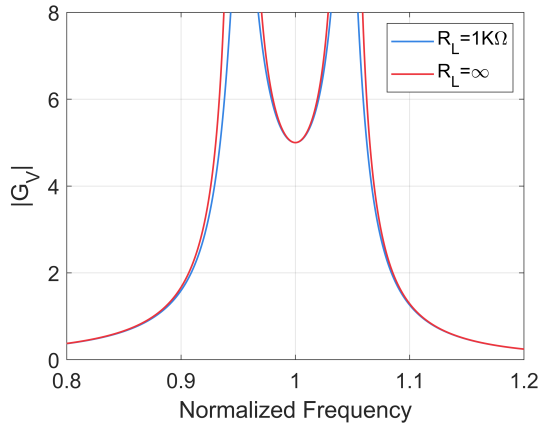

Figure 3. Minimized gain slope by Equation (15)

2.4. Analyzing the Effect of Parasite Resistance

Denote ESR of L_1 as r_1, and likewise r_2, r_{s1} and r_{s2}. The output impedance of the power source is absorbed by r_{s1}. r_{s2} and R_L forms a frequency-independent voltage divider, hence temporarily assume $r_{s2} = 0$ for simplicity. Keep the values of the LC components so that the Equation (4) still stands. The $\mathbf{Z}$ matrix in Equation (1) is re-written as Equation (16).

$$\mathbf{Z} = \begin{pmatrix} jZ_1 + r_{s1} & -\frac{1}{j\omega C_{p11}} & 0 & 0 & 0 \\ -\frac{1}{j\omega C_{p11}} & jZ_2 & -\frac{1}{j\omega C_{p12}} & 0 & 0 \\ 0 & -\frac{1}{j\omega C_{p12}} & jZ_3 + r_1 & -j\omega M & 0 \\ 0 & 0 & -j\omega M & jZ_4 + r_2 & -\frac{1}{j\omega C_{p2}} \\ 0 & 0 & 0 & -\frac{1}{j\omega C_{p2}} & jZ_5 + r_{s2} + R_L \end{pmatrix} \tag{16}$$

 doi:10.20944/preprints202407.0038.v1

Merge Equation (2), (4) and (16). G_{v0}^{-1} with parasite resistance considered is obtained.

$$G_{V0}^{-1} = -\frac{\frac{L_1^2 L_{s2}^2 (r_1+r_{s1})\omega_0^4}{R_L} + L_{s1}^2 M^2 \omega_0^4 + L_1^2 r_2 r_{s1}\omega_0^2 + L_{s1}^2 r_1 r_2 \omega_0^2 - Z_2 Z_4 r_1 r_{s1}}{L_1 L_{s1} L_{s2} M \omega_0^4} \tag{17}$$

$$-j\frac{\frac{L_{s2}^2 Z_2 r_1 r_{s1}\omega_0^2}{R_L} + L_1^2 Z_4 r_{s1}\omega_0^2 + L_{s1}^2 Z_4 r_1 \omega_0^2 + M^2 Z_2 r_{s1}\omega_0^2 + Z_2 r_1 r_2 r_{s1}}{L_1 L_{s1} L_{s2} M \omega_0^4} \tag{18}$$

$$\frac{\mathrm{d}G_{V0}^{-1}}{\mathrm{d}R_L} = -\frac{1}{G_{V0}^2}\frac{\mathrm{d}G_{V0}}{\mathrm{d}R_L} = \frac{L_{s2}}{L_2 L_{s1} M}\left(\frac{r_{s1}}{R_L^2}L_2^2 + \frac{r_1}{R_L^2}L_{s1}^2 + j\frac{r_1 r_{s1}}{\omega_0^2 R_L^2}Z_2\right) \tag{19}$$

Observed from Equation (19), the derivative of G_{V0}^{-1} to R_L is controlled by r_x/R_L. With KΩ-level load and r_x less than 10Ω, the load adjustment rate $\mathrm{d}\left|G_{V0}\right|/\mathrm{dR_L}$ is normally less than 0.1%.

When take r_{s2} into consideration, G_{V0} remains the same except of an extra voltage-division factor $R_L/(R_L + r_{s2})$. L_{s2} usually has a lower Q-factor compared to L_{s1} for the strict size limitation of the implant receiver. However, for a reasonable $Q = 25$ and $L_{s2} = 1\mu$H at 10MHz, $r_{s2} = 2.5\Omega$ is still much smaller than R_L, leading to a division factor of greater than 99.7%. Therefore the voltage gain at ω_0 can still be considered as load-independent.

It is obvious from Equation (18) that G_{V0} is still a single-valued function to k, but is no longer monotonic with parasite resistance. $|G_{V0}|$ first increases with k and then declines after a critical point k_{crit}, which is written as:

$$k_{crit} = \left(\frac{\begin{array}{l} L_2^4 Z_4^2 r_{s1}^2 \omega_0^4 + L_2^4 r_2^2 r_{s1}^2 \omega_0^4 + 2L_2^2 L_{s1}^2 Z_4^2 r_1 r_{s1}\omega_0^4 + 2L_2^2 L_{s1}^2 r_1 r_2^2 r_{s1}\omega_0^4 \\ +L_{s1}^4 Z_4^2 r_1^2 \omega_0^4 + L_{s1}^4 r_1^2 r_2^2 \omega_0^4 + Z_2^2 Z_4^2 r_1^2 r_{s1}^2 + Z_2^2 r_1^2 r_2^2 r_{s1}^2 \end{array}}{L_1^2 L_2^2 \left(L_{s1}^4 \omega_0^8 + Z_2^2 r_{s1}^2 \omega_0^4\right)}\right)^{1/4} \tag{20}$$

The intermediate derivation is omitted for simplicity. From Equation (20), The CV control is made easier as the gain around k_{crit} becomes smoother.

Additionally, for I_{10} which is used to extract k, r_{s2} is indivisible from R_L. Equation (7) is re-written as:

$$\frac{\mathrm{d}I_{10}}{\mathrm{d}R_L} = -\frac{L_1^2 L_{s1}^2 L_{s2}^2 M^2 \omega_0^8}{\left(\begin{array}{l} L_{s1}^2 M^2 R_L \omega_0^4 + L_1^2 L_{s2}^2 r_{s1}\omega_0^4 + L_{s1}^2 L_{s2}^2 r_1 \omega_0^4 + L_1^2 R_L r_2 r_{s1}\omega_0^2 \\ +L_{s1}^2 R_L r_1 r_2 \omega_0^2 - R_L Z_2 Z_4 r_1 r_{s1} + jL_{s2}^2 Z_2 r_1 r_{s1}\omega_0^2 + jL_1^2 R_L Z_4 r_{s1}\omega_0^2 \\ +jL_{s1}^2 R_L Z_4 r_1 \omega_0^2 + jM^2 R_L Z_2 r_{s1}\omega_0^2 + jR_L Z_2 r_1 r_2 r_{s1} \end{array}\right)^2} \tag{21}$$

With r_1, r_2 and r_{s1} join the denominator, I_{10} becomes less sensitive to R_L.

In conclusion, the impact of parasite resistance on resonant frequency and k estimation is negligible in practice. While the exact number of G_V does change, it can be easily tracked with experiment measurement and numerical simulation. Moreover, r_2 is irrelevant to the resonant frequency, allowing a relatively low Q-value for the receiving coil.

2.5. Design Procedure

The circuit in Figure 1b has seven parameters to be determined. Given that the effect of the parasite resistance is limited, the circuit can be assumed as ideal when select the LC values. Based on experiment result, iteration may be needed to account for parasite parameters, including the stray capacitance of the coils.

The coil L_1 and L_2 should be determined before designing the LCC compensation circuit. The parasite parameters of coils and their coupling coefficient range is then measured. The last 5 components can be solved by Equation (4),(5) and (15) to make the circuit resonant at ω_0, smoothen the gain slope and acquire desired gain at k_0. The actual capacitors are selected as

 doi:10.20944/preprints202407.0038.v1

$C'_{p1} = C_{p11} + C_{p12} + C_{coil1}$ and $C'_{p2} = C_{p2} + C_{coil2}$. A numerical simulation based on Equation (3) to check weather the desired gain is achieved. when not, L_{s2}/L_{s1} and the corresponding resonant capacitor must be adjusted. If the adjusted value is beyond acceptance, then roll-back to the coil designing.

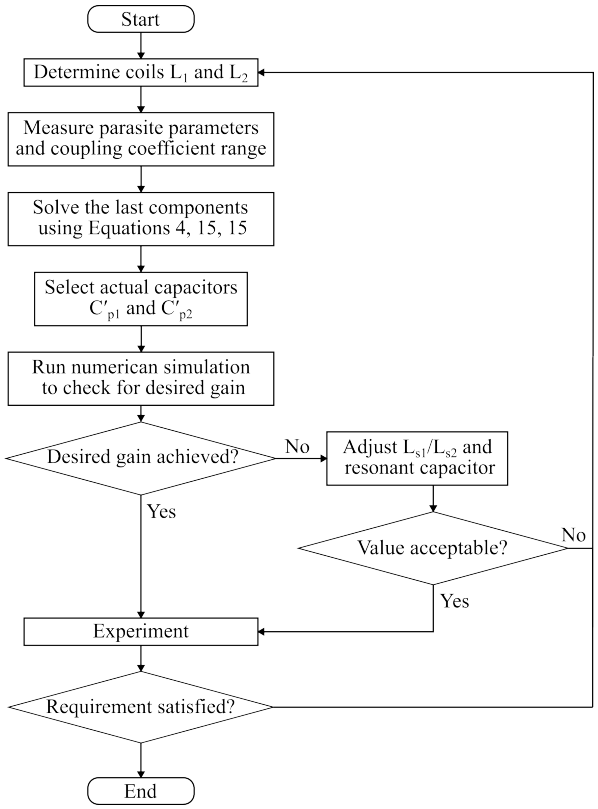

Figure 4. Design flowchart

3. Results

3.1. Validation of LCL-Compensated WPT and Voltage Gain Estimation

An experiment platform of LCL-Compensated WPT circuit that works on 6.78MHz ISM band is constructed, shown in Figure 5. The coils are implemented on FR4 PCBs and of circular shape. The detailed parameters are listed in Table 1 and 2. To adjust the coupling coefficient, i.e. the distance between the coils, the PCBs are fixed on a 3D-printed PLA material base, with the length of the nylon columns between them adjustable.

The transmitter is driven by signal generator via SMA cable. As 0805 chip inductors are used in the compensation circuit, the driving voltage is set to 300mVpp. V_m and V_{out} are monitored by oscilloscope. To cover the internal resistance of the signal generator, V_{in} is also monitored, and V_m data is normalized as V_m/V_{in}.

Two sets of data are recorded in experiment, with $1K\Omega$ pure resistive load and open-circuit respectively. The recorded result and theoretical $V_m - |G_V|$ curves are plotted in Figure 6.

 doi:10.20944/preprints202407.0038.v1

Table 1. Parameters of the PCB coil

Parameter	Value
Outer diameter	44.8mm
Inner diameter	8.6mm
Number of turns	32
Wire width	40mil (1.016mm)
Wire thickness	1.37mil (0.0348mm)[1]
Wire spacing	5mil (0.127mm)
Board thickness	1.6mm

[1] 1 Oz copper.

Table 2. Parameters of the experiment circuit

Component	Value
L_1	22.2μH [1]
L_2	22.3μH [1]
L_{s1}	14.7μH [1]
L_{s2}	5.64μH [1]
C_{coil1}	15pF [2]
C_{coil2}	15pF [2]
C_{p1}	59.9pF [1]
C_{p2}	93.8pF [1]
r_{s1}	35.0Ω [2]
r_{s2}	12.6Ω [2]
r_1	3.24Ω [1]
r_2	3.31Ω [1]

[1] Measured by LCR meter at 100kHz. [2] Measured by VNA at 6.78MHz.

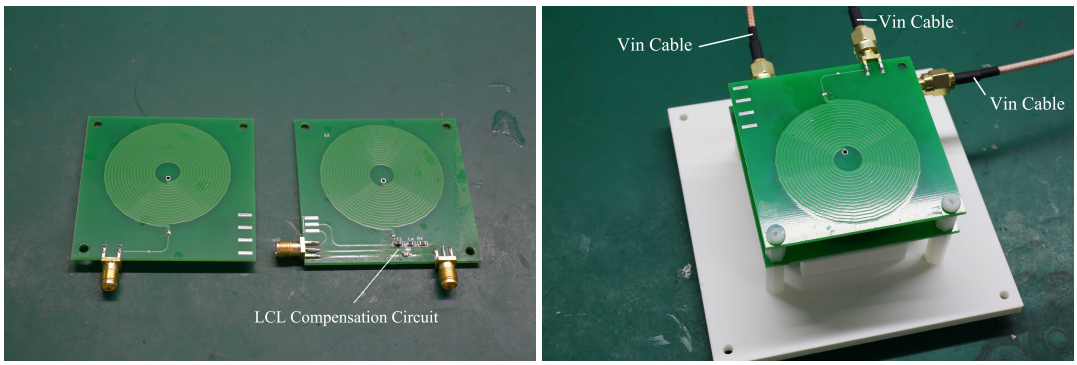

(a) **(b)**

Figure 5. Experiment PCBs(a) and 3D-printed base(b)

Preprints.org (www.preprints.org) | NOT PEER-REVIEWED | Posted: 1 July 2024 doi:10.20944/preprints202407.0038.v1

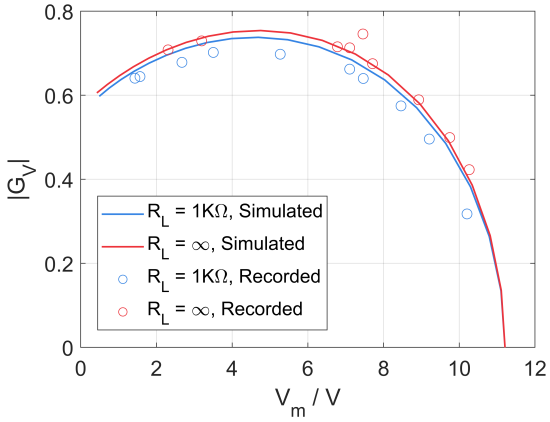

Figure 6. Simulated and recorded V_m-G_V of the experiment circuit, with parameters in Table 2

4. Discussion

4.1. Discussion of experiment result

The recorded data in Figure 6 shows that the $V_m - G_V$ characteristic of experiment circuit follows the identical trend as that of the mathematical model proposed in section 2. The effect of load changes on the G_V estimation is limited, but still observable. Data points of $1K\Omega$ load deviate from the theoretical curve farther, as the parasite parameters vary at the frequency higher than those at which they were measured.

Noises occurred in the measurement has affected the recorded data, creating inconsistent points. Such noises are expected to appear in applications as well. Averaging may be required to ensure the accuracy of the G_V estimation. Additionally, as the independency of resonant voltage gain is slightly weaker than expected due to complex parasite parameters, V_m should be measured during intervals of transmission with lower V_{in}, based on Equation (7). The new estimation strategy is shown in Figure 7.

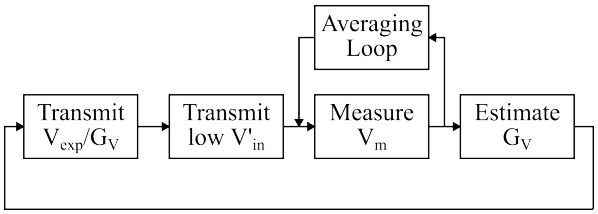

Figure 7. CV-WPT with G_V estimation strategy

4.2. Application

The proposed CV-WPT strategy is planned to be implemented in an implant neural stimulating system shown in Figure 8. To achieve bipolar current stimulation, the system uses amplitude modulation (AM) to transfer power. A threshold voltage is established in the implant stimulator. When the demodulated AM signal surpasses the threshold, the stimulator outputs positive current and vice versa. This procedure is referred as Polarity Recovery. The aforementioned CV-WPT techniques provides robust and precise control with varying k. We use a linear transmission circuit built by Direct Digital Synthesis (DDS) and High-Power Output Current Feedback Amplifier (CFA) for better accuracy, with a trade-off of efficiency.

 doi:10.20944/preprints202407.0038.v1

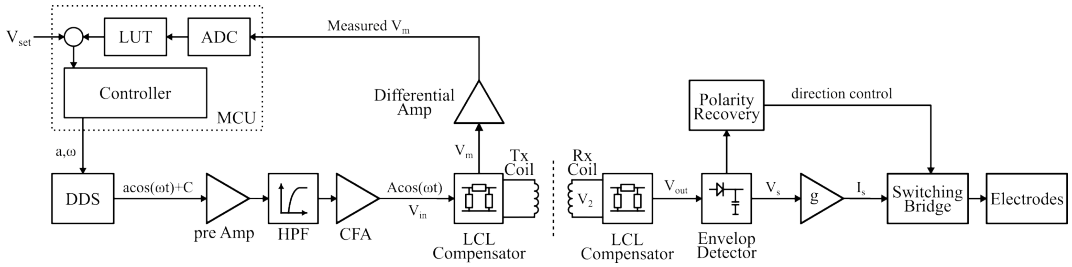

Figure 8. Functional diagram of proposed wireless stimulation system

The MCU uses two LUTs to estimate the received voltage. First of them is derived from Equation (11), it estimates $\hat{k}$ basing on measured V_m. The other is derived from Equation (18) and outputs the corresponding $\hat{G}_V$ of given $\hat{k}$. The desired V_{in} is calculated by $V_{in} = V_{set}/\hat{G}_V$, and sent to the DDS. The intermediate $\hat{k}$ is also used to detect misalignment or fault.

5. Conclusion

The LCL-Compensated WPT circuit is re-analysis for constant voltage transmission. The proposed CV-WPT system uses voltage measures on the transmitting side to estimate the coupling coefficient and voltage gain. Its feasibility is proved and the load-independent characteristic is validated through experiment. Compared to existing methods, our approach does not require frequency sweep or bulky components such as RF relays. The tuning strategy helps further shrink the size of the implant receiver.

Author Contributions: Conceptualization, Zhiyang Cao, Shicong Gui, Chujia Xu and Yubo Li; Formal analysis, Zhiyang Cao; Investigation, Chujia Xu, Rui Zhong and Zhaotan Lin; Project administration, Yubo Li; Resources, Yubo Li; Software, Rui Zhong and Zhaotan Lin; Supervision, Yubo Li; Validation, Zhiyang Cao; Writing – original draft, Zhiyang Cao; Writing – review & editing, Shicong Gui. All authors have read and agreed to the published version of the manuscript.

Funding: This research was funded by Key R&D Program of Zhejiang Province grant number 2022C03038; BLB19J014.

Data Availability Statement: The data presented in this study are available on request. Please connect the corresponding author.

Acknowledgments: We gratefully acknowledge the support and collaboration of Qizhen Taichi Medical Co, Ltd.

Conflicts of Interest: The authors declare no conflicts of interest.

References

1. Haerinia, M.; Shadid, R. Wireless Power Transfer Approaches for Medical Implants: A Review. *1*, 209–229. Number: 2 Publisher: Multidisciplinary Digital Publishing Institute, doi:10.3390/signals1020012.
2. Niu, W.Q.; Chu, J.X.; Gu, W.; Shen, A.D. Exact Analysis of Frequency Splitting Phenomena of Contactless Power Transfer Systems. *60*, 1670–1677. doi:10.1109/TCSI.2012.2221172.
3. Feng, H.; Cai, T.; Duan, S.; Zhao, J.; Zhang, X.; Chen, C. An LCC-Compensated Resonant Converter Optimized for Robust Reaction to Large Coupling Variation in Dynamic Wireless Power Transfer. *63*, 6591–6601. Conference Name: IEEE Transactions on Industrial Electronics, doi:10.1109/TIE.2016.2589922.
4. Xiao, C.; Cheng, D.; Wei, K. An LCC-C Compensated Wireless Charging System for Implantable Cardiac Pacemakers: Theory, Experiment, and Safety Evaluation. *33*, 4894–4905. Conference Name: IEEE Transactions on Power Electronics, doi:10.1109/TPEL.2017.2735441.
5. Li, S.; Li, W.; Deng, J.; Nguyen, T.D.; Mi, C.C. A Double-Sided LCC Compensation Network and Its Tuning Method for Wireless Power Transfer. *64*, 2261–2273. Conference Name: IEEE Transactions on Vehicular Technology, doi:10.1109/TVT.2014.2347006.
6. Wang, X.; Xu, J.; Mao, M.; Ma, H. An LCL-Based SS Compensated WPT Converter With Wide ZVS Range and Integrated Coil Structure. *68*, 4882–4893. Conference Name: IEEE Transactions on Industrial Electronics, doi:10.1109/TIE.2020.2989707.

7. Gupta, R.; Samanta, S. A Novel Parameter Tuning for *LCL–LCL* WPT With Combined CC/CV Charging and Improved Harmonic Performance. pp. 1–11. doi:10.1109/TIE.2024.3363750.
8. Abou Houran, M.; Yang, X.; Chen, W. Magnetically Coupled Resonance WPT: Review of Compensation Topologies, Resonator Structures with Misalignment, and EMI Diagnostics. *7*, 296. Number: 11 Publisher: Multidisciplinary Digital Publishing Institute, doi:10.3390/electronics7110296.
9. Yang, C.L.; Chang, C.K.; Lee, S.Y.; Chang, S.J.; Chiou, L.Y. Efficient Four-Coil Wireless Power Transfer for Deep Brain Stimulation. *65*, 2496–2507. Conference Name: IEEE Transactions on Microwave Theory and Techniques, doi:10.1109/TMTT.2017.2658560.
10. Jiang, D.; Cirmirakis, D.; Schormans, M.; Perkins, T.A.; Donaldson, N.; Demosthenous, A. An Integrated Passive Phase-Shift Keying Modulator for Biomedical Implants With Power Telemetry Over a Single Inductive Link. *11*, 64–77. Conference Name: IEEE Transactions on Biomedical Circuits and Systems, doi:10.1109/TBCAS.2016.2580513.
11. Chen, Q.; Wong, S.C.; Tse, C.K.; Ruan, X. Analysis, Design, and Control of a Transcutaneous Power Regulator for Artificial Hearts. *3*, 23–31. Conference Name: IEEE Transactions on Biomedical Circuits and Systems, doi:10.1109/TBCAS.2008.2006492.
12. Li, J.; Zhang, X.; Tong, X. Research and Design of Misalignment-Tolerant LCC–LCC Compensated IPT System With Constant-Current and Constant-Voltage Output. *38*, 1301–1313. Conference Name: IEEE Transactions on Power Electronics, doi:10.1109/TPEL.2022.3201124.
13. Yao, L.; Zhao, J.; Li, P.; Liu, X.; Xu, Y.P.; Je, M. Implantable stimulator for biomedical applications. 2013 IEEE MTT-S International Microwave Workshop Series on RF and Wireless Technologies for Biomedical and Healthcare Applications (IMWS-BIO), pp. 1–3. doi:10.1109/IMWS-BIO.2013.6756160.
14. Kim, J.D.; Sun, C.; Suh, I.S. A proposal on wireless power transfer for medical implantable applications based on reviews. 2014 IEEE Wireless Power Transfer Conference, pp. 166–169. doi:10.1109/WPT.2014.6839592.
15. Beh, T.C.; Kato, M.; Imura, T.; Oh, S.; Hori, Y. Automated Impedance Matching System for Robust Wireless Power Transfer via Magnetic Resonance Coupling. *60*, 3689–3698. Conference Name: IEEE Transactions on Industrial Electronics, doi:10.1109/TIE.2012.2206337.